A&A, 695, A212 (2025)
https://doi.org/10.1051/0004-6361/202453259

Astronomy & Astrophysics

The EDIBLES survey

X. The 6196 Å diffuse interstellar band: Identification of side DIBs as an indication of a small carrier molecule

A. Ebenbichler[1,⋆], M. Ončák[2], N. Przybilla[1], H. R. Hrodmarsson[3], J. V. Smoker[4,5], R. Lallement[6], A. Farhang[7], C. Bhatt[8,9], J. Cami[8,9,10], M. Cordiner[11,12], P. Ehrenfreund[13], N. L. J. Cox[14], J. Th. van Loon[15], and B. Foing[13,16,17]

[1] Universität Innsbruck, Institut für Astro- und Teilchenphysik, Technikerstr. 25/8, 6020 Innsbruck, Austria
[2] Universität Innsbruck, Institut für Ionenphysik und Angewandte Physik, Technikerstr. 25, 6020 Innsbruck, Austria
[3] Univ Paris Est Creteil and Université Paris Cité, CNRS, LISA, 75013 Paris, France
[4] European Southern Observatory, Alonso de Cordova 3107, Vitacura, Santiago, Chile
[5] UK Astronomy Technology Centre, Royal Observatory, Blackford Hill, Edinburgh EH9 3HJ, UK
[6] GEPI, Observatoire de Paris, PSL Research University, CNRS, Université Paris-Diderot, Sorbonne Paris Cité, Place Jules Janssen, 92195 Meudon, France
[7] School of Astronomy, Institute for Research in Fundamental Sciences, 19395-5531 Tehran, Iran
[8] Department of Physics and Astronomy, The University of Western Ontario, London, ON N6A 3K7, Canada
[9] Institute for Earth and Space Exploration, The University of Western Ontario, London, ON N6A 3K7, Canada
[10] SETI Institute, 189 Bernardo Ave, Suite 100, Mountain View, CA 94043, USA
[11] Astrochemistry Laboratory, NASA Goddard Space Flight Center, Code 691, 8800 Greenbelt Road, Greenbelt, MD 20771, USA
[12] Department of Physics, The Catholic University of America, Washington, DC 20064, USA
[13] Laboratory for Astrophysics, Leiden Observatory, Leiden University, PO Box 9513, 2300 RA Leiden, The Netherlands
[14] Centre d'Etudes et de Recherche de Grasse, ACRI-ST, Av. Nicolas Copernic, Grasse 06130, France
[15] Lennard-Jones Laboratories, Keele University ST5 5BG, UK
[16] ESTEC, ESA, Keplerlaan 1, 2201 AZ Noordwijk, The Netherlands
[17] LUNEX EMMESI Euromoonmars Earth Space Innovation, SBIC Noordwijk, The Netherlands

Received 2 December 2024 / Accepted 5 February 2025

ABSTRACT

Context. Numerous studies of diffuse interstellar band (DIB) profiles have detected substructures, which in turn suggests that large molecules are acting as their carriers. However, some of the narrowest DIBs generally do not show such substructures, suggesting the possibility of very small carriers.

Aims. Based on the previously found tight correlation of the three narrow DIBs at 6196, 6440, and 6623 Å and the present detection of weaker side DIBs to each of them in the extensive dataset from the ESO Diffuse Interstellar Bands Large Exploration Survey, we investigated whether they may stem from small linear carrier molecules. This approach can lead to concrete DIB carrier suggestions, which can be tested in laboratory measurements in future studies.

Methods. We suggest that the DIBs we studied here represent individual rotational transitions of a small molecule. We determined the molecular constants from observations and compared them with data from a large set of quantum-chemical calculations to constrain possible carrier candidates. Furthermore, we determined the rotational temperatures by fitting line ratios using the fitted molecular models.

Results. We determined molecular constants for three DIB systems and the corresponding transition types. The fitted rotational temperatures lie within the range of known interstellar diatomic molecules. We identified several DIB carrier candidates, almost all of them molecular ions. Some of them are metastable species, indicating the possibility of collision complexes as DIB carriers.

Conclusions. If our hypothesis holds, this would be a major step towards the identification of a carrier molecule of the 6196 Å DIB, the strongest among the narrow DIBs.

Key words. ISM: clouds – ISM: lines and bands – ISM: molecules

1. Introduction

Identifying the carriers of the diffuse interstellar bands (DIBs) has been a challenge of astrophysics for many years, since their first discovery more than a century ago (Heger 1922). To date, the number of known DIBs has increased to more than 600, covering spectral features ranging in wavelength from the optical blue (e.g. Hobbs et al. 2009) to the near-infrared (near-IR; e.g. Fan et al. 2022; Ebenbichler et al. 2022; Hamano et al. 2022). Despite considerable efforts in laboratory spectroscopy, their carriers remain elusive, with the exception of C_{60}^+, which gives rise to four DIBs in the near-IR (e.g. Campbell et al. 2015; Spieler et al. 2017; Cordiner et al. 2019; Linnartz et al. 2020). Consequently, more than 99% of the DIBs still lack an identified carrier molecule.

⋆ Corresponding author; Alexander.Ebenbichler@uibk.ac.at

However, numerous laboratory, theoretical, and observational investigations have yielded insights into potential DIB carriers. Due to their wavelength stability, it is believed that DIBs are caused by molecules in the gas phase (Herbig 1995). Observations indicate that the nature of these molecules can be of a wide variety. Some very broad DIBs show a Lorentzian profile shape, for example the 4430 (Snow 2002) and 5450 Å DIB. In the case of the 5450 Å DIB, an acetylene (C_2H_2) plasma absorption spectrum coincided in wavelength, band width, and band shape (Linnartz et al. 2010). Unfortunately, the carrier that formed in the plasma could not be unambiguously identified in that work due to the short lifetime of the transition of $\tau \approx 0.15$ ps, but it certainly contains hydrogen and carbon. Many classes of molecules have been investigated as possible carriers, such as carbon chain radicals (Motylewski et al. 2000), cationic carbon rings of various lengths (Rademacher et al. 2022), or polycyclic aromatic hydrocarbons (PAHs; Salama et al. 1999; Cox 2011), also in specific shapes, such as polyacenes (Omont et al. 2019). In the current state of research, large, carbonaceous molecules are suspected to cause most of the DIBs. This hypothesis is supported by the frequent observation of substructures in band profiles, which is generally attributed to unresolved rotational bands of heavy molecules (Cossart-Magos & Leach 1990; Ehrenfreund & Foing 1996; Edwards & Leach 1993; Cami et al. 2004; MacIsaac et al. 2022; Bhatt et al. 2025), the higher stability of large molecules against UV radiation, and the size of the only known DIB carrier C_{60}^+.

However, more recent work has begun to explore the possibility of smaller molecules containing transition metals as potential DIB carriers (Juanes et al. 2024), potentially in cationic form. The idea of small molecules in the interstellar medium (ISM) might be valid and worthwhile to follow up as the first molecules found in the optical spectra of the diffuse ISM such as CH (Dunham 1937; Swings & Rosenfeld 1937), CN (McKellar 1940), and CH^+ (Douglas & Herzberg 1941) are diatomic. At the same time, studies of molecular ions have been carried out less frequently in the laboratory, but ionisation is ubiquitous in view of the radiation field permeating the diffuse ISM. The search for small diatomic or maybe triatomic DIB carrier molecules has a significant advantage over the identification of larger molecules, which is due to their more thorough investigability using state-of-the-art quantum-chemical modelling. It allows us to compute (although still approximately) the properties of the ground and excited electronic states of almost any pair of atoms. This allows us to determine the properties of small DIB carriers to a very precise level if we are able to interpret interstellar spectra correctly. As the nature of DIB carriers is still uncertain, it is important to keep in mind that the carriers probably represent a range in sizes, lifetimes, symmetries, and charges, calling for different approaches to determine the carriers responsible for each DIB class.

In this work, we explore the possibility of small, probably diatomic molecules acting as carriers of some narrow DIBs, derived purely from observational indicators. In Sect. 2, we introduce our spectroscopic dataset and the observational indicators, leading to the idea of small DIB carrier molecules. In Sect. 3, we describe the methods we used for calculating molecular parameters and synthetic spectra of the carriers. Based on this, we derive molecular constants and rotational temperatures in Sect. 4, and in Sect. 5 we discuss the validity of the results and the differences to previous hypotheses.

2. Observations

2.1. Observational data

For this work, we used the homogeneous high-quality observational data from the ESO Diffuse Interstellar Bands Large Exploration Survey (EDIBLES; Cox et al. 2017). The dataset consists of spectra acquired using the Ultraviolet and Visual Echelle Spectrograph (UVES; Dekker et al. 2000) on the Very Large Telescope UT-2 at the European Southern Observatory (ESO) at Paranal, Chile. These spectra cover 123 sight lines towards Galactic O- and B-type stars. Four different instrumental set-ups were used using the blue and red arms of UVES with a dichroic mirror to achieve a near-complete wavelength coverage between approximately 3050 and 10 420 Å. The spectral resolving power was high, with $R = \lambda/\Delta\lambda \approx 70\,000$–$110\,000$, utilising 0.4″ (blue) and 0.3″ (red) slits. The EDIBLES survey used custom procedures based on the UVES pipeline to fully reduce and calibrate the data, achieving very high signal-to-noise ratio (S/N) values of ∼1000 for the final data products (see Cox et al. (2017) for details on target selection, observing strategy, and data reduction).

2.2. New observational findings

In Paper VIII of the EDIBLES publication series (Ebenbichler et al. 2024), several families of DIBs with correlating band strength and profile shapes were identified from an analysis of the entire sight line sample, called DIB profile families. In that paper it was concluded that DIBs of the same profile families are probably caused by the same molecules or by chemically closely related molecules.

A closer inspection of the clustering analysis from Paper VIII in the vicinity of the three 6196 Å DIB profile family members (the 6196, 6440, and 6623 Å DIBs) shows that they are accompanied by weaker DIBs, only a few wave numbers apart from the central DIBs. Those DIBs were selected by our DIB alignment algorithm, due to their similar profile shapes compared to the 6196 Å DIB. This pattern was detected in a statistically significant number of sight lines, which is visualised in the histograms of Fig. 1, where the median strength pattern of the components is also shown, relative to the 6196 Å DIB[1]. The information on these DIBs is summarised in Table 1, which gives for each of the three central DIBs the names of the individual component DIBs, the mean wave number $\tilde{\nu}$, the mean shift towards the respective central DIB $\Delta\tilde{\nu}$, the corresponding wavelength of the transition in air $\lambda_{\rm air}$, and finally the intensity ratio I and the band strength Pearson correlation coefficient r relative to the 6196 Å DIB. The radial velocities of the side and main DIBs correlate, which is indicated by the similar widths of the histograms in Fig. 1. Only for the 6440 Å DIB can a larger spread be seen, which is expected because of the blend with another DIB. Detection of the accompanying side DIBs strongly depends on the S/N of the sight line spectra, as they can become very weak, down to a few percent of the strength of the 6196 Å DIB. We note in anticipation of later insights that a very strong correlation of these band profiles

[1] The 6196 Å DIB is the strongest among narrow DIBs, easily identifiable even in mildly reddened sight lines, and one of the few DIBs that have been identified in other galaxies such as M31 or M33 (Cordiner et al. 2008a,b).

Table 1. DIB alignment results of the three DIB systems.

Main DIB	DIB name	$\tilde{\nu}$ (cm^{-1})	$\Delta\tilde{\nu}$ (cm^{-1})	λ_{air} (Å)	I	r
6196	6195	16 138.4 ± 0.1	3.2 ± 0.1	6194.68 ± 0.03	0.15 ± 0.04	0.909
	6196	16 135.2 ± 0.1	...	6195.93 ± 0.03	1.00 ± 0.06	0.998
	6199	16 127.4 ± 0.1	−7.8 ± 0.1	6198.92 ± 0.05	0.05 ± 0.03	0.649
6440	6438	15 528.2 ± 0.1	3.4 ± 0.2	6438.13 ± 0.04	0.04 ± 0.03	0.795
	6440	15 524.8 ± 0.2	...	6439.51 ± 0.07	0.18 ± 0.10	0.802
	6442	15 517.9 ± 0.2	−6.9 ± 0.2	6442.39 ± 0.06	0.04 ± 0.08	0.173
6623	6622	15 098.0 ± 0.2	2.8 ± 0.2	6621.55 ± 0.07	0.06 ± 0.03	0.868
	6623	15 095.2 ± 0.1	...	6622.78 ± 0.05	0.13 ± 0.02	0.943
	6626	15 088.5 ± 0.1	−6.7 ± 0.2	6625.72 ± 0.05	0.05 ± 0.01	0.922

Notes. Errors are calculated from standard deviations of our DIB alignment results. $\Delta\tilde{\nu}$ denotes the difference in wave numbers between a side DIB and its main DIB.

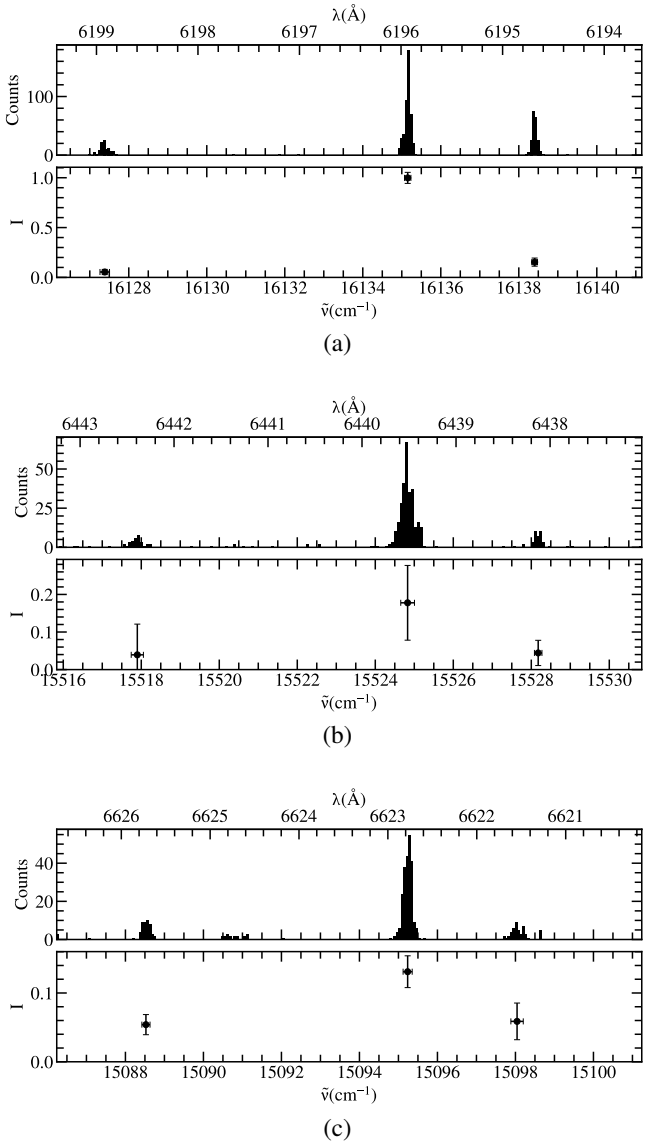

Fig. 1. Histogram (top) and median strength ratios (bottom) of the proposed side band matches of the 6196 (panel a), 6440 (panel b), and 6623 Å DIBs (panel c) from DIB alignment, using the full EDIBLES sample. The strength ratios are relative to the 6196 Å DIB.

with respect to the 6196 Å DIB may not necessarily be expected because of indications for spin-orbit (**LS**) coupling[2] influencing the detailed profile shapes.

From this point on, we concentrate only on a particularly valuable subset of the sight lines covered by the EDIBLES survey, the 12 single-cloud sight lines identified by MacIsaac et al. (2022, their Table 1). Only for these sight lines can one single DIB carrier population with distinct environmental conditions be assumed, an assumption that is necessary for this analysis. All central DIBs considered here and their side DIBs show the same approximately Gaussian profile shape as the 6196 Å DIB in these single-cloud sight lines. An example of the similarity of the three DIB systems is shown for the sight lines towards HD 185418 and HD 185859 in Fig. 2. We note that the 6440 Å DIB is blended with another DIB, giving rise to the double-peak form.

In the following, we consider each of the strong DIBs with their side DIBs as a DIB system. Because of the systematic occurrence of the same pattern in the three DIB systems, this cannot be a coincidence. We therefore assume each DIB system to be caused by one electronic ro-vibrational transition with resolved lines. To our knowledge, this is the first time such a correlation has been found for narrow DIBs, opening up the possibility to derive carrier properties on an observational basis, promising progress in comparison to previous attempts (e.g. Herbig & Leka 1991).

3. Methods

We used customised Python scripts to model the electronic ro-vibrational transitions of linear molecules and fitted them to the observations using the package LMFIT (Newville et al. 2014). Three different kinds of electronic transitions were considered: $\Sigma \rightarrow \Sigma$, $\Sigma \rightarrow \Pi$, and $\Pi \rightarrow \Delta$. The corresponding electronic states have the electronic angular momentum quantum number $\Lambda = 0$ (Σ), $\Lambda = 1$ (Π), and $\Lambda = 2$ (Δ). Assuming these types of transitions, we determined the rotational constants of the electronic ground state X and excited state A using the positions of the three

[2] In molecular physics, the electron angular momentum pertaining to an electronic state in a molecule is denoted with **L**, and the total electronic spin angular momentum with **S**. These differ from the quantum numbers, L and S, which reflect the projection of the vectors **L** and **S** onto the molecular axis.

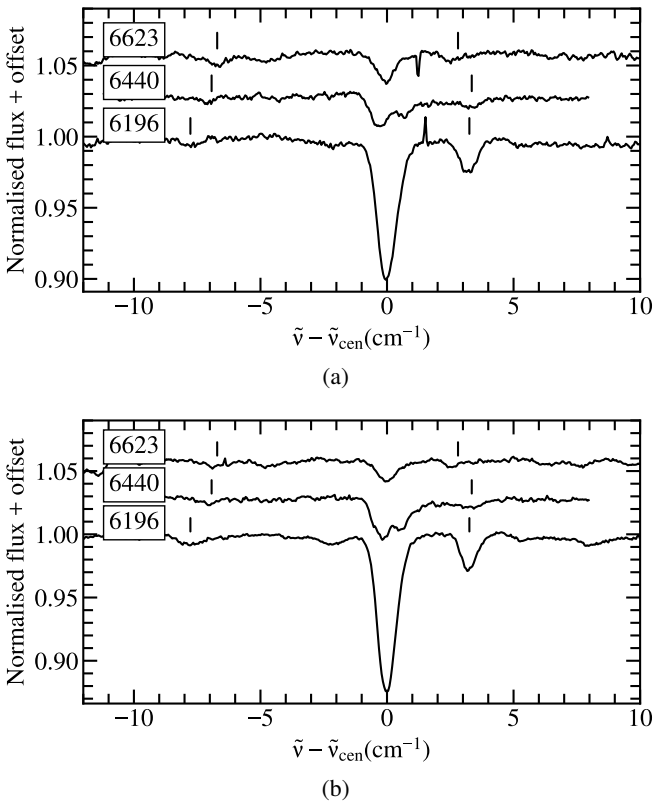

Fig. 2. DIB systems 6196, 6440, and 6623 Å in the HD 185418 (panel a) and HD 185859 (panel b) single-cloud sight lines. The main DIBs are at $\tilde{\nu} = 0$ and the weaker DIBs are indicated by vertical lines. The 6440 Å DIB is blended with another DIB. All systems were shifted to the wave number of the central DIB $\tilde{\nu}_{\rm cen}$.

strongest transitions. We determined the rotational constants B'' and B' for the assumed ground and excited state, respectively, and the wave number of the electronic origin transition $\tilde{\nu}_0$ by evaluating Eq. (1) for the respective values of the total rotational quantum numbers in the ground state (J'') and the excited state (J') of three transitions and solving the resulting system of linear equations. The total angular momentum must always be equal to or greater than the electronic angular momentum in the ground state ($J'' \geq \Lambda''$) and the excited state ($J' \geq \Lambda'$) because it is the sum of the electronic and nuclear angular momenta. There is never a transition directly at ν_0, which would only be the case for the Q(0) transition. For the $\Sigma \rightarrow \Sigma$ transition no Q branch is allowed as $\Lambda' - \Lambda'' = \Delta\Lambda = 0$, and for all the other transitions either Λ'' or Λ' is larger than 0. Equations (2), (3), and (4) apply to the case of a $\Sigma \rightarrow \Sigma$, $\Sigma \rightarrow \Pi$, and $\Pi \rightarrow \Delta$ transition, respectively. The equations may be written as

$$\tilde{\nu}_{J\rightarrow J'} = \tilde{\nu}_0 + B'J'(J'+1) - B''J''(J''+1), \quad (1)$$

$$\begin{pmatrix} 1 & 2 & 0 \\ 1 & 6 & -2 \\ 1 & 0 & -2 \end{pmatrix} \cdot \begin{pmatrix} \tilde{\nu}_0 \\ B' \\ B'' \end{pmatrix} = \begin{pmatrix} \tilde{\nu}_{\rm R(0)} \\ \tilde{\nu}_{\rm R(1)} \\ \tilde{\nu}_{\rm P(1)} \end{pmatrix} = \begin{pmatrix} \tilde{\nu}_{0\rightarrow1} \\ \tilde{\nu}_{1\rightarrow2} \\ \tilde{\nu}_{1\rightarrow0} \end{pmatrix}, \quad (2)$$

$$\begin{pmatrix} 1 & 2 & 0 \\ 1 & 6 & -2 \\ 1 & 2 & -2 \end{pmatrix} \cdot \begin{pmatrix} \tilde{\nu}_0 \\ B' \\ B'' \end{pmatrix} = \begin{pmatrix} \tilde{\nu}_{\rm R(0)} \\ \tilde{\nu}_{\rm R(1)} \\ \tilde{\nu}_{\rm Q(1)} \end{pmatrix} = \begin{pmatrix} \tilde{\nu}_{0\rightarrow1} \\ \tilde{\nu}_{1\rightarrow2} \\ \tilde{\nu}_{1\rightarrow1} \end{pmatrix}, \quad (3)$$

$$\begin{pmatrix} 1 & 6 & -2 \\ 1 & 12 & -6 \\ 1 & 6 & -6 \end{pmatrix} \cdot \begin{pmatrix} \tilde{\nu}_0 \\ B' \\ B'' \end{pmatrix} = \begin{pmatrix} \tilde{\nu}_{\rm R(1)} \\ \tilde{\nu}_{\rm R(2)} \\ \tilde{\nu}_{\rm Q(2)} \end{pmatrix} = \begin{pmatrix} \tilde{\nu}_{1\rightarrow2} \\ \tilde{\nu}_{2\rightarrow3} \\ \tilde{\nu}_{2\rightarrow2} \end{pmatrix}, \quad (4)$$

where $\tilde{\nu}_{J''\rightarrow J'}$ is the wave number of a single ro-vibrational transition from J'' to J'. To calculate the line intensities $I(J'', J')$ of the rotational transitions from J'' to J', we used the equation

$$I(J'', J') \propto A_{\Lambda''J''} n_{J''} = A_{\Lambda''J''}(2J''+1) \exp -\frac{J''(J''+1)B''}{k_B T_{\rm rot}}, \quad (5)$$

where k_B is the Boltzmann constant, $T_{\rm rot}$ is the rotational temperature, and $A_{\Lambda''J''}$ is the Hönl-London factor, as described by Herzberg (1991). For $\Delta\Lambda = +1$, that is the $\Sigma \rightarrow \Pi$ and $\Pi \rightarrow \Delta$ transitions the Hönl-London factors are

$$A_{\Lambda''J''} = \frac{(J''+2+\Lambda'')(J''+1+\Lambda'')}{(J''+1)(2J''+1)} \quad (\text{for } \Delta J = +1), \quad (6)$$

$$A_{\Lambda''J''} = \frac{(J''+1+\Lambda'')(J''-\Lambda'')}{J''(J''+1)} \quad (\text{for } \Delta J = 0), \quad (7)$$

$$A_{\Lambda''J''} = \frac{(J''-1-\Lambda'')(J''-\Lambda'')}{J''(2J''+1)} \quad (\text{for } \Delta J = -1), \quad (8)$$

where J'' and Λ'' are the total angular momentum and the electronic angular momentum in the ground state. In the case of the $\Sigma \rightarrow \Sigma$ transition, where $\Delta\Lambda = 0$, the Hönl-London factors are

$$A_{\Lambda''J''} = \frac{(J''+1+\Lambda'')(J''+1-\Lambda'')}{(J''+1)(2J''+1)} \quad (\text{for } \Delta J = +1), \quad (9)$$

$$A_{\Lambda''J''} = \frac{(J''+\Lambda'')(J''-\Lambda'')}{J''(2J''+1)} \quad (\text{for } \Delta J = -1). \quad (10)$$

In the case $\Delta\Lambda = 0$, $\Delta J = 0$ is not allowed. It should be noted that we assume molecules with an electron spin of $S = 0$, which may be incorrect for many molecule candidates, but serves as a first approximation for the transition strengths. For the final absorption spectrum we used a simple Gaussian as a line profile function and calculated absorption models with a linear continuum. More detailed descriptions for the selection rules, intensity ratios of individual lines, and the $T_{\rm rot}$ sensitivity are presented in Appendix B.

To find carrier candidates with the observed parameters, we performed quantum chemical calculations at the coupled clusters singles and doubles with non-iteratively included triples level with the def2QZVP basis set (CCSD(T)/def2QZVP optimisation of suitable molecules upon CCSD/def2TZVP pre-optimisation of all candidate molecules) to determine the rotational constants of possible diatomic XY (X = H, He; Y = Li–Xe; and X, Y = H–Ne) in different ionisation states with charges from −1 to +2 and spin multiplicity up to octuplet, as well as the $HFHe^+$ ion in the Gaussian software (Frisch et al. 2016). We note that the single-reference treatment of the coupled cluster method is potentially problematic for transition metal complexes, and should be improved upon in following investigations. Transition metal complexes have a challenging electronic structure, and methods based on a single Slater determinant wave function might fail to describe them reliably (Hait et al. 2019). Therefore, calculations using multi-reference methods are desirable (Khedkar & Roemelt 2021). Finally, the most stable molecular term was confirmed through multi-reference configuration interaction (MRCI/def2QZVP) as implemented in Molpro (Werner et al. 2012, 2020). We note that no excitations between states of different spin multiplicity were considered; these might play a significant role in molecules including transition metals. We also did not consider autoionising transitions. Including these effects is outside the scope of this paper as it is a first test of this hypothesis.

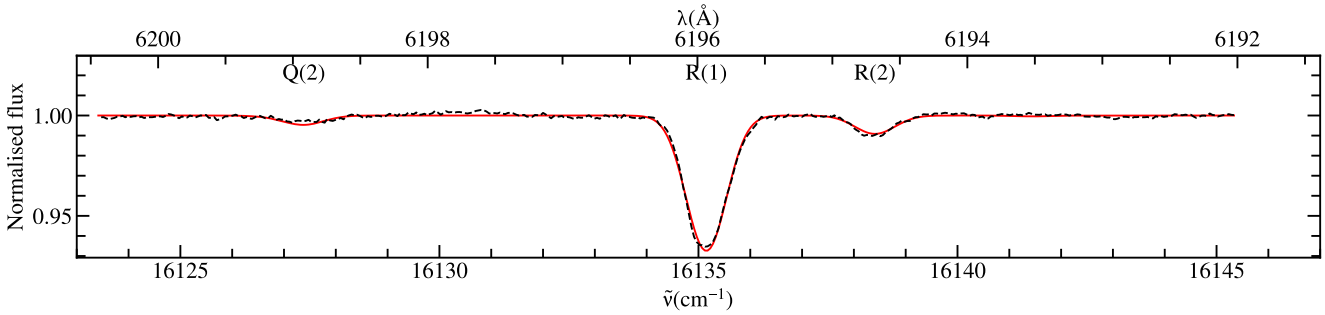

Fig. 3. Fit of the 6196 Å DIB system in the HD 170740 sight line (dashed black) using our $\Pi \rightarrow \Delta$ transition model (red).

Table 2. Rotational constants calculated from DIB alignment results.

Transition	B'' (cm^{-1})	B' (cm^{-1})	$\tilde{\nu}_0$ (cm^{-1})
6196 $\Sigma \rightarrow \Sigma$	2.05 ± 0.07	1.84 ± 0.05	$16\,131.48 \pm 0.10$
6196 $\Pi \rightarrow \Delta$	1.94 ± 0.05	1.84 ± 0.05	$16\,128.01 \pm 0.16$
6623 $\Sigma \rightarrow \Pi$	3.36 ± 0.09	2.38 ± 0.06	$15\,090.48 \pm 0.16$
6440 $\Sigma \rightarrow \Pi$	3.47 ± 0.12	2.57 ± 0.06	$15\,519.69 \pm 0.20$

Notes. Errors are calculated with Gaussian error propagation of the measurement errors in Table 1. An additional approximated systematic error of 0.4 cm^{-1} can be expected to be present, which can be caused by **LS** coupling.

4. Analysis

In the 6196 Å DIB system, the lower-energy DIB is weaker than the central DIB, and the higher-energy DIB is even weaker (Fig. 1a). In order to generate a ro-vibrational transition of this pattern, either an electronic $\Sigma \rightarrow \Sigma$ (Fig. A.1) or a $\Pi \rightarrow \Delta$ (Fig. 3) transition is required. For the 6440 and 6623 Å DIB systems, the side peaks are of equal strengths within the errors (i.e. $I(6438) = I(6442)$, $I(6622) = I(6626)$), but weaker than the central DIB (see Figs. 1b and 1c, or Table 1). This pattern can only be reproduced by an electronic $\Sigma \rightarrow \Pi$ transition, where $I(\mathrm{R}(1)) = I(\mathrm{Q}(1))$. We determined the molecular constants for each transition scenario by solving the linear Eqs. (2), (3), and (4) for the transitions listed in Table 1. The results are shown in Table 2, which lists B'', B', and $\tilde{\nu}_0$ for the four transition scenarios investigated. The systematic errors are derived from the standard deviations of the DIB alignment results, and a systematic error is caused by possible **LS** coupling, as described below.

As a test of our ro-vibrational transition model, we fitted the 6196 and 6623 Å DIBs and their respective side bands using the molecular model only by varying the rotational temperature T_{rot}, the width of a Gaussian profile σ, and the radial velocity RV for our single-cloud sight lines. The 6440 Å DIB could not be fully investigated because of its strong blend with another DIB. However, considering the determined line ratios, that is two equally strong secondary DIBs, the most probable transition type is a $\Sigma \rightarrow \Pi$ transition, just as for the 6623 Å DIB system. The results of the 6196 Å DIB system are shown in Table 3 and of the 6623 Å DIB system in Table 4. The (discarded) results of the 6196 Å DIB system for a $\Sigma \rightarrow \Sigma$ transition are shown in Table A.1 together with a plot of the fit in the HD 170740 sight line in Fig. A.1. We show our adopted fit for the HD 170740 sight line for the 6196 Å DIB system in Fig. 3 and for the 6623 Å DIB system in Fig. 4. The other fits for our single-cloud sight lines are shown in Figs. C.1, C.2, and C.3. We note that the other five sight lines have S/N values that are too low to be analysed for the 6623 Å DIB system. The use of a Gaussian profile is sufficient for our purpose in describing the individual components. The next weaker rotational components R(3) and Q(3) are too weak to be detectable in any sight line.

For the 6196 Å DIB system, our data had the necessary S/N to perform an additional analysis of the DIB profile shapes.

Table 3. Fit results of the 6196 Å DIB system using a $\Pi \rightarrow \Delta$ transition model.

Sight line	T_{rot} (K)	σ ($km\,s^{-1}$)	RV ($km\,s^{-1}$)
HD 23180	4.96 ± 0.15	7.71 ± 0.10	12.56 ± 0.09
HD 24398	5.86 ± 0.13	7.45 ± 0.08	13.20 ± 0.08
HD 144470	4.55 ± 0.21	8.79 ± 0.14	-9.66 ± 0.14
HD 147165	4.05 ± 0.34	9.86 ± 0.24	-7.67 ± 0.24
HD 147683	5.27 ± 0.21	8.02 ± 0.14	-0.99 ± 0.14
HD 149757	5.27 ± 0.23	9.63 ± 0.18	-14.53 ± 0.18
HD 166937	4.46 ± 0.13	7.68 ± 0.08	-6.34 ± 0.08
HD 170740	5.24 ± 0.07	7.16 ± 0.04	-11.37 ± 0.04
HD 184915	5.38 ± 0.15	6.88 ± 0.09	-12.62 ± 0.08
HD 185418	5.83 ± 0.12	6.95 ± 0.07	-9.02 ± 0.07
HD 185859	5.62 ± 0.09	6.48 ± 0.05	-8.50 ± 0.05
HD 203532	4.52 ± 0.16	7.27 ± 0.09	13.94 ± 0.09

Notes. The radial velocity (RV) is measured in the barycentric rest frame.

Table 4. Fit results of the 6623 Å DIB system using a $\Sigma \rightarrow \Pi$ transition model.

Sight line	T_{rot} (K)	σ ($km\,s^{-1}$)	RV ($km\,s^{-1}$)
HD 23180	5.47 ± 1.03	6.03 ± 0.91	14.40 ± 0.87
HD 24398	6.43 ± 0.62	10.12 ± 0.86	13.32 ± 0.79
HD 170740	6.11 ± 0.25	7.94 ± 0.28	-11.01 ± 0.27
HD 184915	6.09 ± 0.58	6.01 ± 0.48	-11.46 ± 0.46
HD 185418	5.50 ± 0.29	6.70 ± 0.29	-7.95 ± 0.28
HD 185859	4.76 ± 0.25	7.20 ± 0.28	-8.35 ± 0.27
HD 203532	6.84 ± 0.74	6.94 ± 0.65	13.61 ± 0.62

Notes. If a sight line is not listed, the fit was not successful due to the low signal-to-noise ratio. RV is measured in the barycentric rest frame.

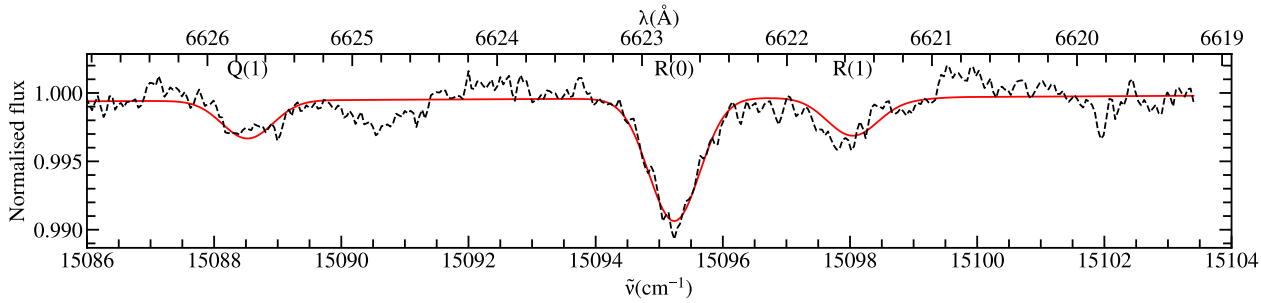

Fig. 4. Fit of the 6623 Å DIB system in the HD 170740 sight line (dashed black) using our $\Sigma \rightarrow \Pi$ transition model (red).

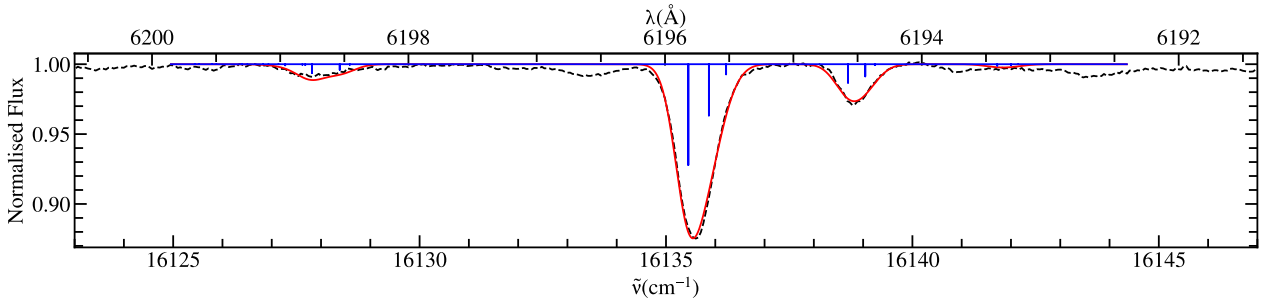

Fig. 5. 6196 Å DIB system in the HD 185859 sight line (dashed black) and a $^2\Pi \rightarrow {}^2\Delta$ transition model including **LS** coupling (red), generated with Pgopher. The unconvolved 'stick' spectrum is shown in blue. This plot shows how **LS** coupling can explain the systematic asymmetry of the 6196 Å DIB.

On closer inspection of the profiles, one finds that the components of the 6196 Å DIB system have asymmetric profile shapes, which is systemic in the single-cloud sight lines. For a $^2\Pi \rightarrow {}^2\Delta$ transition, **LS** coupling (which is expected for such a transition) can explain this asymmetry. We generated a model with Pgopher (Western 2017), using the parameters $B'' = 1.9\,\mathrm{cm}^{-1}$, $B' = 1.8\,\mathrm{cm}^{-1}$, and **LS** coupling constants in the ground (A'') and excited state (A') of $A'' = A' = -0.45\,\mathrm{cm}^{-1}$. Due to the shifts in **LS** coupling, we had to change the rotational constants by $0.4\,\mathrm{cm}^{-1}$ for each electronic level. This is an additional systematic error source of the values in Table 2. As a first approximation, we added a systematic error of $0.4\,\mathrm{cm}^{-1}$ to the statistical error from DIB alignment. The comparison of the model with the 6196 Å DIB system in the HD 185859 sight line is displayed in Fig. 5. The effect of the **LS** coupling has almost the identical effect on the 6195 Å DIB and causes a stronger split for the 6199 Å DIB. This **LS** coupling improves the fit overall and can explain the systematically asymmetric profile shape of the DIB system. We abstained from implementing and fitting a detailed molecular model with **LS** coupling and leave this qualitative explanation for the profile shapes, as the overall picture will be little changed.

With this hypothesis, supported by the observed molecular constants and the types of electronic transitions, we searched for appropriate carrier candidates for our three DIB systems. We compared the rotational constants of stable molecules calculated in Gaussian with our observations in Table 2. If the theoretical value matched the observation within 20% and the relative energy of the respective electronic state was within 0.6 eV with respect to the tentative most stable spin multiplicity, we checked if the molecule candidates had excited states above the ground state with an energy difference close to the origin wave number $\tilde{\nu}_0$, that is in the 1.5–3 eV region, as well as the required symmetry of the molecular terms. We also excluded some molecules and ions for which experimental measurements already provided rotational constants or excitation energies incompatible with those given in Table 2. The resulting candidates are listed in Table 5.

Table 5. Rotational constants of proposed carrier molecules as calculated at the CCSD(T)/def2QZVP level, along with the most stable molecular term as determined at the MRCI/def2QZVP level.

Molecule	B'' (cm^{-1})	Molecular ground term	Lit.
(NO^{2+})	1.93	$^2\Sigma^+$	o [(a)]
($HFHe^+$)	1.94	$^2\Pi$	...
KH^-	2.99	$^2\Sigma^+$	...
SrH^-	3.31	$^1\Sigma^+$	...
SrH	3.66	$^2\Sigma^+$	f [(b)]
(CrH^+)	3.74	$^7\Sigma^+$	o [(c)]
CaH^-	3.85	$^1\Sigma^+$	...

Notes. References: [(a)]Baková et al. (2008); [(b)]Liu et al. (2016); [(c)]Romero et al. (2022). Molecules in the top part are candidates for the 6196 Å DIB system; molecules in the bottom part are candidates for the other two systems. The species in brackets are metastable. In the last column (Lit.), molecules marked with 'f' are ruled out as carriers, '...' marks the absence of literature, and 'o' marks molecules for which there is literature available, but the carrier is neither confirmed nor ruled out.

5. Discussion

5.1. Previous interpretations of the 6196 Å DIB

The assumption of a small polar molecule as the carrier of the 6196 Å DIB is a strong contradiction to previous work, which assumed a large carrier molecule, due to the presence of substructures. This relies on the finding of two subpeaks

separated by ~8 km s^{-1} in the 6196 Å DIB towards the Sco OB2 association (Galazutdinov & Krełowski 2023). This substructure was interpreted as potential PR-branches of a very large molecule with a very small rotational constant B. However, a study of neutral hydrogen by Sancisi (1974) finds an expanding H I shell associated with Sco OB2, which could be the result of an old supernova remnant, slowed down by interaction with the ISM. Its expansion speed is 3 km s^{-1} in each direction. The observed substructures could therefore simply be different velocity components of the same carrier concentrated on the shell rim, traversed twice by the line of sight. Kaźmierczak et al. (2009) report a correlation between the rotational temperature of interstellar C_2 and the full width at half maximum of the 6196 Å DIB, indicating that the DIB is caused by a large molecule and shows unresolved rotational bands. However, the sample size is too small to be certain about the correlation, and more importantly the 6196 Å DIB is a σ DIB, so its carrier resides in very different cloud environments than C_2. Hence, this correlation must be taken with caution.

However, the substructure could not be systematically confirmed in the EDIBLES single-cloud sight lines at $R \approx 110\,000$, unlike in the case for the 5797, 6397, or 6614 Å DIBs (MacIsaac et al. 2022). We fitted a double Gaussian to the 6196 Å DIB and inspected the residuals to see small-scale structures. We did not find any intrinsic patterns that exceed the noise level, which is illustrated in Fig. C.4. In addition, no substructure of the 6196 Å DIB was found initially at an instrumental resolution of 0.075 Å, which equates to $R = \lambda/\Delta\lambda \approx 80\,000$ (Smith et al. 1981), which was confirmed by Herbig & Soderblom (1982).

In other work, DIB studies on the Herschel 36 sight line found no substructure (Oka et al. 2013), but extended red wings for multiple DIBs, also for the 6196 Å DIB. This finding is in conflict with the hypothesis of a large carrier molecule showing rotational splitting because the temperature in the Herschel 36 sight line is assumed to be rather high and does not show splitting. The extended red wings can be explained by the Doppler shift as well, since strong dynamics and large redshifts of ~80 km s^{-1} of H_2 in the vicinity of Herschel 36 were observed by Rachford et al. (2014). The red wings may not be visible in other molecules and ionised species because they reside in different areas of the ISM. These dynamics could also influence the DIB structure in this particular sight line. In summary, it has not been unambiguously proven that the 6196 Å DIB shows systematic substructure, so the possibility of a smaller molecular carrier should not be ignored.

5.2. A new paradigm for the 6196 Å DIB

In a change of approach, we assume that the profile of the 6196 Å DIB and of its profile family members are purely caused by Doppler shifts. The fitted Doppler width of $\sigma \approx 7$ km s^{-1} is considerably larger than the Doppler width of most known interstellar atomic and molecular lines. An explanation for this phenomenon might be that those DIB carriers might not be stable against elastic collisions, which are needed to reduce the turbulent velocity dispersion in interstellar gases. The carriers would only exist with velocity dispersion originating from their production, a velocity dispersion that can never narrow down. Hence, this would imply a continuous formation and destruction of DIB carriers. The perceived velocity distribution could be caused during the production of the carrier molecule, which may be influenced by the high levels of turbulence in the diffuse ISM. The 6196 Å DIB is strongly correlated with the 6614 Å DIB (McCall et al. 2010), for which Bhatt et al. (2025) reported correlating line widths with CH^+. According to Godard et al. (2023), CH^+ is the consequence of mass exchanges between the cold neutral medium (CNM) and the warm neutral medium (WNM), induced by large-scale turbulence and thermal instability, indicating that large line widths are likely caused by turbulent environments. We expect a variable line width of the 6196 Å DIB across different sight lines due to this effect. The timescale of the formation destruction cycle of the carrier could be comparable to CH^+ (Godard et al. 2023, their Table 2), but at this point we are not able to provide reliable estimates. A molecular broadening mechanism such as lifetime broadening is very unlikely, because of the sharpness of some subfeatures in the 'split' sight lines towards the Sco OB2 association. Moreover, we focus on each DIB system as a whole, rather than specifically trying to explain the detailed profile shape of the 6196 Å DIB itself.

The determined molecular constants point to small linear molecules as the carriers of the investigated DIB systems. Because of the large rotational constant, most likely they are diatomic, possibly triatomic. Due to the different B'', the 6196 Å DIB system must have a different carrier than the other two, while the 6440 and 6623 Å DIB systems could have the same carrier. The fitted rotational temperatures (Tables 3, 4 and A.1) show consistently low temperatures of less than 7 K, making polar molecules much more likely than nonpolar carriers. For the 6196 Å DIB system, the $\Sigma \rightarrow \Sigma$ transition model shows rotational temperatures below the CMB temperature for all of our single-cloud sight lines. Such low temperatures are very unlikely. A polar molecule should have at least the CMB temperature of $T_{\rm CMB} = 2.7260 \pm 0.0013$ K (Fixsen 2009) because the CMB is the strongest radiation source in the diffuse ISM at radio wavelengths (see e.g. Draine 2011, Chapter 12). The $\Pi \rightarrow \Delta$ model shows rotational temperatures $T_{\rm rot} > T_{\rm CMB}$ for all sight lines, as well as the fits for the 6623 Å DIB system. The $T_{\rm rot}$ values of the 6196 and 6623 Å DIB systems do not correlate with each other, but both range between 4 and 7 K. These temperatures are close to the known rotational temperatures of interstellar polar diatomics. Measurements of CO in the UV range by Wannier et al. (1982) show a rotational temperature of CO of $T_{\rm rot} = 4$ K in the HD 149757 (ζ Oph) sight line. It is a promising outcome of our analysis that we determine rotational temperatures in this range for a candidate polar diatomic carrier.

The search for such a carrier proved to be difficult. Only a handful of diatomics showed rotational constants in the right ranges and additionally have the right electronic states to match our observations (see Table 5). The list contains a doubly ionised molecule, which seems very exotic at first sight, but this scenario should not be discarded in the harsh ISM environment. Although the doubly ionised species are only metastable against dissociation, we still list them as candidates because they can still cause DIBs if their abundance is high enough. It might be possible that some DIB carriers are short-lived, but are produced at a sufficient rate because many molecules cannot survive the harsh interstellar radiation field. Hence, collision complexes could be possible carriers of some DIBs.

Furthermore, we also consider the abundances of the constituents of the molecules to assess whether they may exist in sufficient quantities to produce the observed DIBs. We use the present-day cosmic abundances (Nieva & Przybilla 2012; Przybilla et al. 2008, 2013), supplemented by solar abundances (e.g. Asplund et al. 2021) for the missing species.

A candidate in Table 5 is NO^{2+}, but it has a Σ ground state, and the excited electronic state closest to 16 130 cm^{-1} is a Π state (Baková et al. 2008), which is incompatible with our observations of the 6196 Å DIB system. However, the $A^2\Pi$ state is expected to be heavily blended with the $X^2\Sigma$ state from simple considerations of energetic proximity and perturbation selection rules. The biggest caveat with this methodology is that it does not account for the nuances in the excited states themselves, namely that of state mixings or perturbations. Technically, this means that we cannot completely discount NO^{2+} on the basis of this argument, especially since nitrogen and oxygen are both amongst the most abundant elements with $\epsilon(N) = \log(N/H) + 12 = 7.79 \pm 0.04$ and $\epsilon(O) = 8.76 \pm 0.05$.

We found no studies regarding possible interstellar abundances for KH^-, SrH^-, or CaH^-, and we can only discuss the abundances of the heavy molecular components. Potassium and calcium are quite abundant ($\epsilon(K) = 5.08 \pm 0.04$, $\epsilon(Ca) = 6.29 \pm 0.03$), which means that some amount of both molecular anions may be present in the ISM. Strontium is rather rare ($\epsilon(Sr) = 2.88 \pm 0.03$), but it is among the first-peak elements of the s-process. Consequently, the circumstellar envelopes' asymptotic giant branch (AGB) may be the formation sites of the neutral molecules favoured by the enhanced s-process abundances and generally higher densities there, later to be further processed in the ISM.

SrH is one of the most intensely studied molecules in our candidate list. Both experimental and theoretical measurements (Liu et al. 2016) disagree with our observed ground-state rotational constant, and thus confirm that SrH can be excluded as a candidate due to a mismatch of rotational constants and electronic energy levels. Although it is probably metastable with a relative energy of about 1 eV, one interesting candidate is CrH^+, because molecular CrH has been observed in sunspots (Engvold et al. 1980), S-type stars (Lindgren & Olofsson 1980), and brown dwarfs (Kirkpatrick et al. 1999). In a theoretical study, Romero et al. (2022) found that CrH^+ can be formed by electron ionisation of CrH, whereas the cation has a smaller ionisation cross-section than the neutral. It was also found that CrH^+ is dissociated upon recombination with an electron, making it more stable in ISM regions of very low density, such as the DIB environment. The abundance of Cr is also rather high ($\epsilon(Cr) = 5.63 \pm 0.02$), making CrH^+ more likely as a carrier. Generally, metal-hydride cations could be good candidates as similar molecules have been detected in the ISM, such as ArH^+ (Barlow et al. 2013). For completeness, we examined deuteride molecules and ions as candidates, which provide a larger number of candidate carriers than hydride ions, but which can be expected to be significantly rarer because of the low deuterium-to-hydrogen ratio. The discussion can be found in Appendix D. The anions HK^-, SrH^-, and CaH^- are not intuitive because of their negative charge, but they should not be excluded because of this argument.

As one of the tri-atomic carrier candidates, $HFHe^+$ has a rotational constant that is very close to our observed value for the 6196 Å DIB. This complex is metastable, and would have to be prepared in an excited state before fluorescing to the ground state, but HF has been found to be abundant at the edge of interstellar clouds, for example in the Orion Bar (Kavak et al. 2019). HF should be the dominant reservoir of interstellar fluorine, due to the exothermic reaction $H_2 + F \rightarrow HF + H$. Consequently, $HF + He^+ \rightarrow HFHe^+$ could be formed. In theoretical studies, the interaction of (HF^+) and He has been studied on multiple occasions because of the significance of HF in laser physics. The newest study by Nakbi et al. (2024) concludes that the configuration $FHHe^+$ is more strongly bound than $HFHe^+$ and also has a much smaller B''. This is consistent with previous studies, as shown by Schmelz & Rosmus (1994) and Lotrich et al. (2004). However, HF is abundant at the edge of the Orion Bar, coinciding with the skin-effect[3] phenomenon of DIBs. This makes $HFHe^+$ a good candidate from the observational point of view.

Using white dwarfs and Extreme Ultraviolet Explorer (EUVE) data, Wolff et al. (1999) found that He is significantly ionised within the first one hundred parsecs around the Sun, with $He^+/(He + He^+) \approx 40\%$. This high degree of ionisation was recently confirmed, at least for the nearby clouds, on the basis of the interstellar flow within the Solar System (Bzowski et al. 2019). Recently, Güsten et al. (2019) have detected HeH^+ in a planetary nebula. Some evidence of helium-containing DIB carriers might even have been observed in the laboratory in plain sight by Linnartz et al. (2010). Unfortunately, the carrier could not be unambiguously identified in that work, due to the short lifetime of the transition of $\tau \approx 0.15$ ps, but it certainly contains hydrogen and carbon. As a standard procedure, but interestingly in this context, a 1% C_2H_2/He mixture was used for the experiment. Normally, He is assumed to not react with other elements or molecules, but in a plasma it could be ionised, thus opening up several reaction channels. This would explain the absence of the feature without a plasma. Given the high abundance of He in the ISM, a significant fraction should be ionised to He^+, especially in the presumably extreme DIB environment, potentially forming cationic molecules with other abundant atoms.

6. Conclusions

In this work we have shown that there is a consistent pattern of the 6196, 6440, and 6623 Å DIBs and their respective weaker side DIBs. The hypothesis of rotational bands being the cause is a first approach to explaining these patterns and supplies a list of specific small carrier molecule candidates that are testable with more detailed theoretical calculations, with additional observations, and finally in the laboratory. Other mechanisms that are able to cause this pattern, such as spin-orbit coupling, should also be addressed in future studies. In the coming years, the computational precision in quantum chemistry will only increase, giving us the possibility to search for small carrier candidates more precisely. In broader theoretical studies of diatomic and maybe triatomic molecules, it should be possible to determine a DIB carrier with the information shown here. To investigate this hypothesis further, detailed profile fitting of whole DIB systems has to be implemented, which will constrain additional molecular constants and clarify whether the hypothesis is valid. If such small DIB carriers exist, they should have rotational transitions in the electronic ground state as well. Comprehensive searches for such transitions in the radio, in emission, or in absorption are necessary. In this work we have shown that small molecules could very well be good DIB carrier candidates, with many observational indicators supporting this assumption. We want to emphasise the idea of collision complexes as possible DIB carrier candidates such as $HFHe^+$. Because of the extreme conditions in the diffuse ISM, chemical processing could be enhanced, possibly leading to abundances of such complexes that are high enough to become observable. It is important for the progress in DIB research to keep an open mind concerning all possible theories.

[3] Many DIBs – especially σ type – are primarily found along the edge or skin of interstellar clouds. This is known as the skin-effect.

Acknowledgements. A.E. and N.P. gratefully acknowledge support from the Austrian Science Fund FWF, Grant DOI 10.55776/W1259 (DK-ALM). JC acknowledges support from an NSERC Discovery Grant. This article/publication is based upon work from COST Action CA21126 – Carbon molecular nanostructures in space (NanoSpace), supported by COST (European Cooperation in Science and Technology). This work is based on observations collected at the European Organisation for Astronomical Research in the Southern Hemisphere under ESO programme 194.C-0833. Data are publicly available through the ESO Science Archive Facility at `http://archive.eso.org/eso/eso_archive_main.html`. The computational results presented were achieved using the HPC infrastructure LEO of the University of Innsbruck.

References

Appelblad, O., & Barrow, R. F. 1984, Phys. Scr, 29, 456
Asplund, M., Amarsi, A. M., & Grevesse, N. 2021, A&A, 653, A141
Baková, R., Fišer, J., Šedivcová-Uhlíková, T., & Špirko, V. 2008, J. Chem. Phys., 128, 144301
Barlow, M. J., Swinyard, B. M., Owen, P. J., et al. 2013, Science, 342, 1343
Bhatt, C., Cami, J., Sarre, P. J., et al. 2025, ACS Earth Space Chem., 9, 227
Black, J. H., & Dalgarno, A. 1973, ApJ, 184, L101
Bzowski, M., Czechowski, A., Frisch, P. C., et al. 2019, ApJ, 882, 60
Cami, J., Salama, F., Jiménez-Vicente, J., Galazutdinov, G. A., & Krełowski, J. 2004, ApJ, 611, L113
Campbell, E. K., Holz, M., Gerlich, D., & Maier, J. P. 2015, Nature, 523, 322
Cordiner, M. A., Cox, N. L. J., Trundle, C., et al. 2008a, A&A, 480, L13
Cordiner, M. A., Smith, K. T., Cox, N. L. J., et al. 2008b, A&A, 492, L5
Cordiner, M. A., Linnartz, H., Cox, N. L. J., et al. 2019, ApJ, 875, L28
Cossart-Magos, C., & Leach, S. 1990, A&A, 233, 559
Cox, N. L. J. 2011, EAS Publ. Ser., 46, 349
Cox, N. L. J., Cami, J., Farhang, A., et al. 2017, A&A, 606, A76
Dekker, H., D'Odorico, S., Kaufer, A., Delabre, B., & Kotzlowski, H. 2000, in Proc. SPIE, 4008, Optical and IR Telescope Instrumentation and Detectors, eds. M. Iye, & A. F. Moorwood, 534
Douglas, A. E., & Herzberg, G. 1941, ApJ, 94, 381
Draine, B. T. 2011, Physics of the Interstellar and Intergalactic Medium (Princeton, NJ: Princeton University Press)
Dunham, T., J. 1937, PASP, 49, 26
Ebenbichler, A., Postel, A., Przybilla, N., et al. 2022, A&A, 662, A81
Ebenbichler, A., Smoker, J. V., Lallement, R., et al. 2024, A&A, 686, A50
Edwards, S. A., & Leach, S. 1993, A&A, 272, 533
Ehrenfreund, P., & Foing, B. H. 1996, A&A, 307, L25
Engvold, O., Woehl, H., & Brault, J. W. 1980, A&AS, 42, 209
Fan, H., Schwartz, M., Farhang, A., et al. 2022, MNRAS, 510, 3546
Fixsen, D. J. 2009, ApJ, 707, 916
Frisch, M. J., Trucks, G. W., Schlegel, H. B., et al. 2016, Gaussian~16 Revision A.03 (Wallingford, CT: Gaussian Inc.)
Galazutdinov, G. A., & Krełowski, J. 2023, MNRAS, 523, 4158
GharibNezhad, E., Shayesteh, A., & Bernath, P. F. 2012, J. Mol. Spectrosc., 281, 47
Ghazizadeh, E., & Shayesteh, A. 2017, J. Mol. Spectrosc., 339, 17
Godard, B., Pineau des Forêts, G., Hennebelle, P., Bellomi, E., & Valdivia, V. 2023, A&A, 669, A74
Güsten, R., Wiesemeyer, H., Neufeld, D., et al. 2019, Nature, 568, 357
Hait, D., Tubman, N. M., Levine, D. S., Whaley, K. B., & Head-Gordon, M. 2019, J. Chem. Theory Computat., 15, 5370
Hamano, S., Kobayashi, N., Kawakita, H., et al. 2022, ApJS, 262, 2
Heays, Alan N., Visser, R., Gredel, R., et al. 2014, A&A, 562, A61
Heger, M. L. 1922, Lick Obs. Bull., 10, 141
Herbig, G. H. 1995, ARA&A, 33, 19
Herbig, G. H., & Leka, K. D. 1991, ApJ, 382, 193
Herbig, G. H., & Soderblom, D. R. 1982, ApJ, 252, 610
Herzberg, G. 1991, Molecular Spectra and Molecular Structure, reprint ed. with corrections edn. (Malabar (Fla.): Krieger)
Hobbs, L. M., York, D. G., Thorburn, J. A., et al. 2009, ApJ, 705, 32
Juanes, M., Jin, S., Saragi, R. T., et al. 2024, J. Phys. Chem. A, 128, 1306
Kavak, Ü., van der Tak, F. F. S., Tielens, A. G. G. M., & Shipman, R. F. 2019, A&A, 631, A117
Kaźmierczak, M., Gnaciński, P., Schmidt, M. R., et al. 2009, A&A, 498, 785
Khedkar, A., & Roemelt, M. 2021, Phys. Chem. Chem. Phys., 23, 17097
Kirkpatrick, J. D., Allard, F., Bida, T., et al. 1999, ApJ, 519, 834
Lakshminarayana, G., & Shetty, B. 1987, J. Mol. Spectrosc., 122, 417
Lemoine, B., Demuynck, C., Destombes, J. L., & Davies, P. B. 1988, J. Chem. Phys., 89, 673
Lindgren, B., & Olofsson, G. 1980, A&A, 84, 300
Linnartz, H., Wehres, N., van Winckel, H., et al. 2010, A&A, 511, L3
Linnartz, H., Cami, J., Cordiner, M., et al. 2020, J. Mol. Spectrosc., 367, 111243
Liu, X., Liang, G., Zhang, X., Xu, H., & Yan, B. 2016, J. Quant. Spectr. Rad. Transf., 170, 169
Lotrich, V. F., Wormer, P. E. S., & van der Avoird, A. 2004, J. Chem. Phys., 120, 93
MacIsaac, H., Cami, J., Cox, N. L. J., et al. 2022, A&A, 662, A24
McCall, B. J., Drosback, M. M., Thorburn, J. A., et al. 2010, ApJ, 708, 1628
McKellar, A. 1940, PASP, 52, 187
Motylewski, T., Linnartz, H., Vaizert, O., et al. 2000, ApJ, 531, 312
Nakbi, H., Bejaoui, M., Ghanmi, C., Alharzali, N., & Berriche, H. 2024, J. Quant. Spec. Radiat. Transf., 328, 109168
Newville, M., Stensitzki, T., Allen, D. B., & Ingargiola, A. 2014, `https://doi.org/10.5281/zenodo.11813`
Nieva, M. F., & Przybilla, N. 2012, A&A, 539, A143
Oka, T., Welty, D. E., Johnson, S., et al. 2013, ApJ, 773, 42
Omont, A., Bettinger, H. F., & Tönshoff, C. 2019, A&A, 625, A41
Przybilla, N., Nieva, M. F., & Butler, K. 2008, ApJ, 688, L103
Przybilla, N., Nieva, M. F., Irrgang, A., & Butler, K. 2013, EAS Publ. Ser., 63, 13
Rachford, B. L., Snow, T. P., & Ross, T. L. 2014, ApJ, 786, 159
Rademacher, J., Reedy, E. S., & Campbell, E. K. 2022, J. Phys. Chem. A, 126, 2127
Ram, R. S., & Bernath, P. F. 1995, J. Mol. Spectrosc., 172, 91
Romero, J., Limão-Vieira, P., & Probst, M. 2022, J. Phys. Condens. Matter, 34, 374001
Salama, F., Galazutdinov, G. A., Krełowski, J., Allamandola, L. J., & Musaev, F. A. 1999, ApJ, 526, 265
Sancisi, R. 1974, in Galactic Radio Astronomy, 60, eds. F. J. Kerr, & S. C. Simonson, 115
Schmelz, T., & Rosmus, P. 1994, Chem. Phys. Lett., 220, 117
Smith, W. H., Cochran, W. D., Snow, T. P., & Jura, M. 1981, ApJ, 248, 128
Snow, T. P. 2002, ApJ, 567, 407
Spieler, S., Kuhn, M., Postler, J., et al. 2017, ApJ, 846, 168
Swings, P., & Rosenfeld, L. 1937, ApJ, 86, 483
Wannier, P. G., Penzias, A. A., & Jenkins, E. B. 1982, ApJ, 254, 100
Werner, H.-J., Knowles, P. J., Knizia, G., Manby, F. R., & Schütz, M. 2012, WIREs Comp. Mol. Sci., 2, 242
Werner, H.-J., Knowles, P. J., Manby, F. R., et al. 2020, J. Chem. Phys., 152, 144107
Western, C. M. 2017, J. Quant. Spec. Radiat. Transf., 186, 221
Wolff, B., Koester, D., & Lallement, R. 1999, A&A, 346, 969

Appendix A: Discarded Σ → Σ transition model for the 6196 Å DIB system

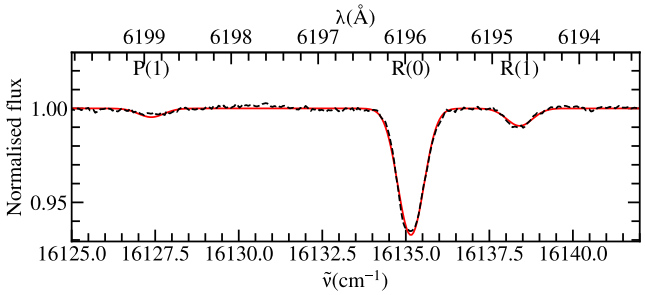

Fig. A.1. 6196 Å DIB and its companions in the single cloud sight line towards HD 170740 (dashed black) compared with a synthetic spectrum (in red) of a Σ → Σ transition of a linear molecule with $T_{\rm rot}$ = 2.18 ± 0.02 K.

Table A.1. Fit results for the single cloud dominated 6196 Å DIB sightlines using a Σ → Σ transition model.

Sight line	$T_{\rm rot}$ (K)	σ (km s^{-1})	RV (km s^{-1})
HD23180	2.08 ± 0.05	7.707 ± 0.097	12.56 ± 0.09
HD24398	2.41 ± 0.04	7.456 ± 0.079	13.20 ± 0.08
HD144470	1.94 ± 0.07	8.791 ± 0.144	−9.67 ± 0.14
HD147165	1.76 ± 0.12	9.854 ± 0.244	−7.67 ± 0.24
HD147683	2.18 ± 0.07	8.009 ± 0.140	−0.99 ± 0.14
HD149757	2.20 ± 0.08	9.629 ± 0.181	−14.53 ± 0.17
HD166937	1.90 ± 0.05	7.675 ± 0.082	−6.34 ± 0.08
HD170740	2.18 ± 0.02	7.162 ± 0.043	−11.36 ± 0.04
HD184915	2.22 ± 0.05	6.879 ± 0.085	−12.62 ± 0.08
HD185418	2.37 ± 0.04	6.943 ± 0.067	−9.02 ± 0.07
HD185859	2.31 ± 0.03	6.473 ± 0.049	−8.50 ± 0.05
HD203532	1.93 ± 0.06	7.273 ± 0.094	13.94 ± 0.09

Notes. The resulting rotational temperatures are consistently below the CMB level. RV is measured in the barycentric rest frame.

Appendix B: Rotational model calculations

B.1. Selection rules

For electronic transitions between a lower state X with the electronic orbit quantum number Λ″ and an excited state A with the electronic orbit quantum number Λ′, the electronic orbit quantum number Λ can only change by ΔΛ = Λ′ − Λ″ = ±1 or 0. In addition to the electrons, the nuclei in the molecule can rotate as well. This rotation is characterised by the nuclear rotational quantum number F. The total rotational quantum number is $J = \Lambda + F$. This means that J is always larger than or equal to Λ in the respective state, so $J' \geq \Lambda'$ and $J'' \geq \Lambda''$. The effect of those selection rules for the different electronic transitions is shown in Table B.1.

B.2. Relative line strengths

The different electronic transitions can have different rotational temperatures or relative line strengths. In Fig. B.1 we compare this effect for our used electronic transitions Σ → Σ, Σ → Π and Π → Δ. Σ → Σ and Π → Δ show the same relative line strengths of the three strongest rotational transitions, but the Σ → Σ model needs a much lower $T_{\rm rot}$ to fit the same line ratios as the Π → Δ model. However, both have the common pattern of strong central absorption, weaker absorption at higher wave numbers, and even weaker absorption at lower wave numbers. The Σ → Π is a different case, where the two weaker features R(1) and Q(1) are equally strong. They have the same J'' and the same Hönl-London factors of $A_{\Lambda'' J''} = 1$, which makes them equally strong for all $T_{\rm rot}$ (Fig. B.1).

B.3. Sensitivity to $T_{\rm rot}$

To show the sensitivity of the models with respect to $T_{\rm rot}$, we show a comparison of different rotational temperatures in Fig. B.2. A variation by 0.5 K is roughly equal to 3σ of the fitting errors in Table 3 and causes a change in the model spectrum, which is significant with respect to the S/N of the data. It should be also noted, that we fit the whole spectrum, so we should be able to reach higher sensitivity.

Table B.1. Allowed rotational transitions for the respective electronic transitions.

Electronic transition	$J''_{\rm min}$	$J'_{\rm min}$	Min. J rot. transitions
Σ → Σ	0	0	R(0), P(1)
Σ → Π	0	1	R(0), Q(1), P(2)
Π → Δ	1	2	R(1), Q(2), P(3)

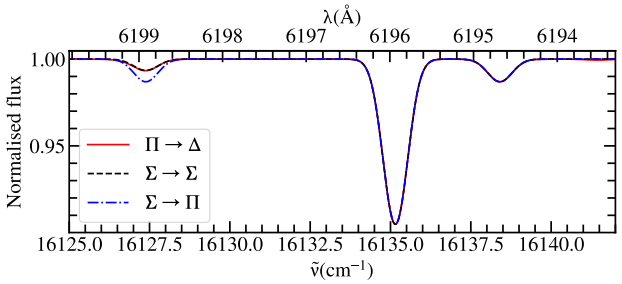

Fig. B.1. Comparison between a Π → Δ (red, $T_{\rm rot}$ = 5.24 K), Σ → Σ (dashed black, $T_{\rm rot}$ = 2.17 K) and Σ → Π (dash-dotted blue, $T_{\rm rot}$ = 4.59 K) transition. The rotational temperatures are matched, so that the models have the same line ratio of the two strongest transitions. In this temperature range, the Π → Δ and Σ → Σ models have the same line ratios, but different temperatures. The Σ → Π model has a stronger transition at lower wave numbers, which is as strong as the weak transition at higher wave numbers.

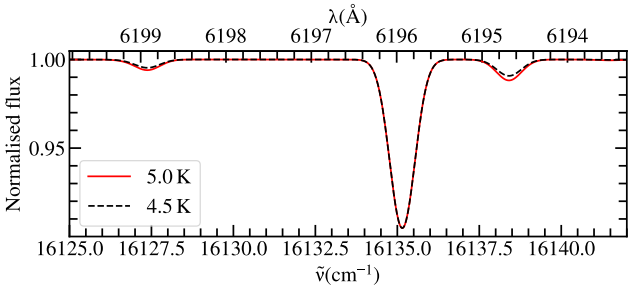

Fig. B.2. Π → Δ model at $T_{\rm rot}$ = 5.0 K (red) and $T_{\rm rot}$ = 4.5 K (dashed black), visualising the sensitivity of the model to changes in $T_{\rm rot}$.

Appendix C: Additional figures

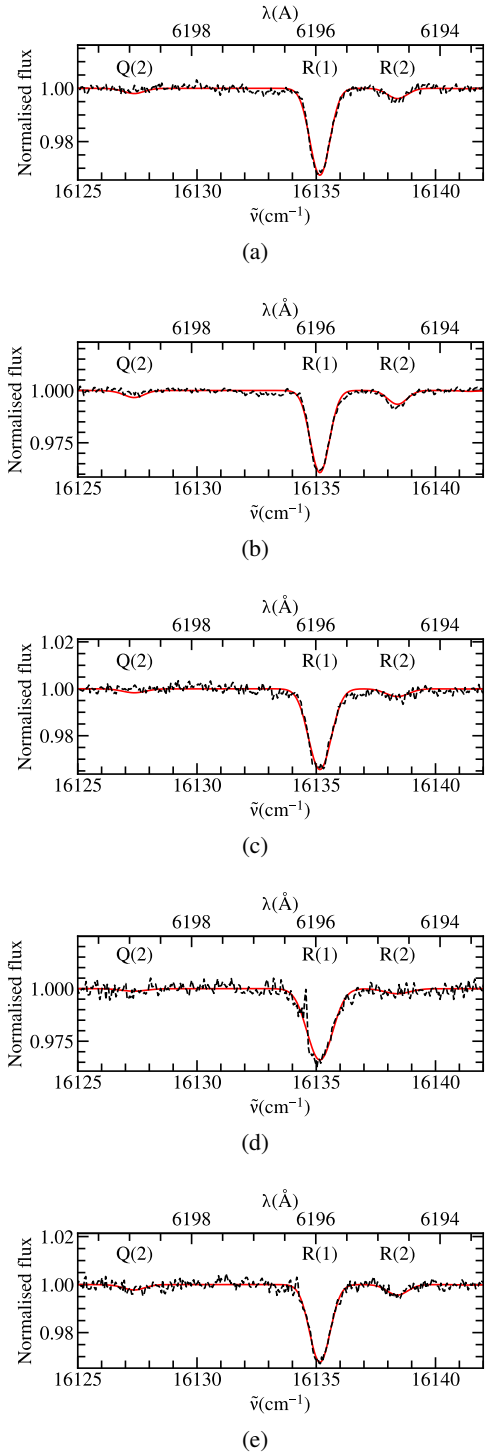

Fig. C.1. Fit of the HD 23180 (a), HD 24398 (b), HD 144470 (c), HD 147165 (d), and HD 147683 (e) sight lines using a $\Pi \rightarrow \Delta$ transition of a linear molecule model for the 6196 Å DIB system.

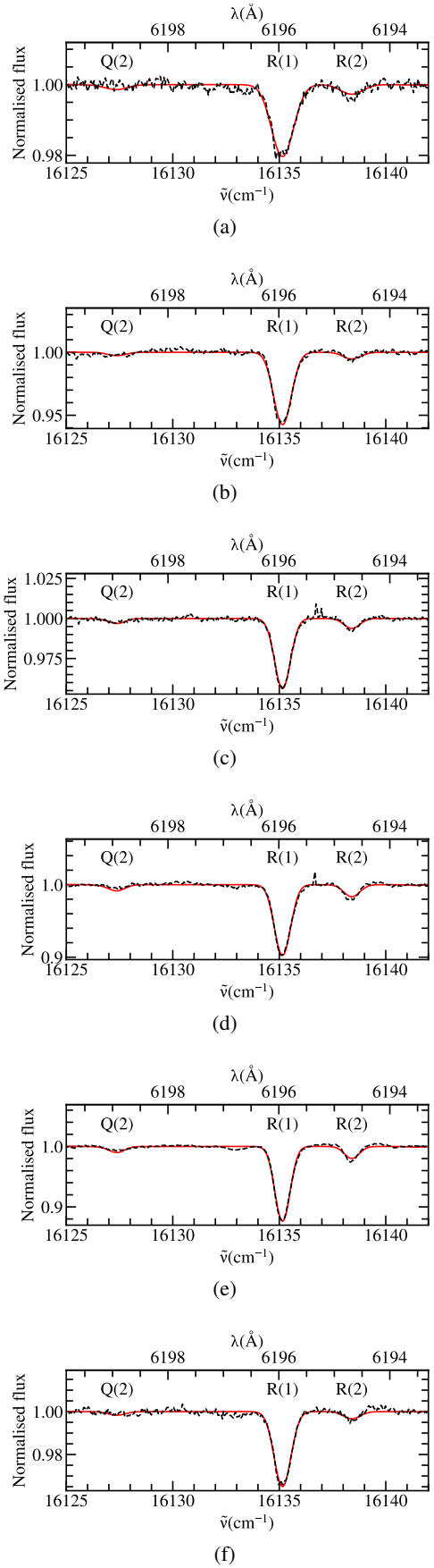

Fig. C.2. Same as Fig. C.1, but for the sight lines towards HD 149757 (a), HD 166937 (b), HD 184915 (c), HD 185418 (d), HD 185859 (e), and HD 203532 (f).

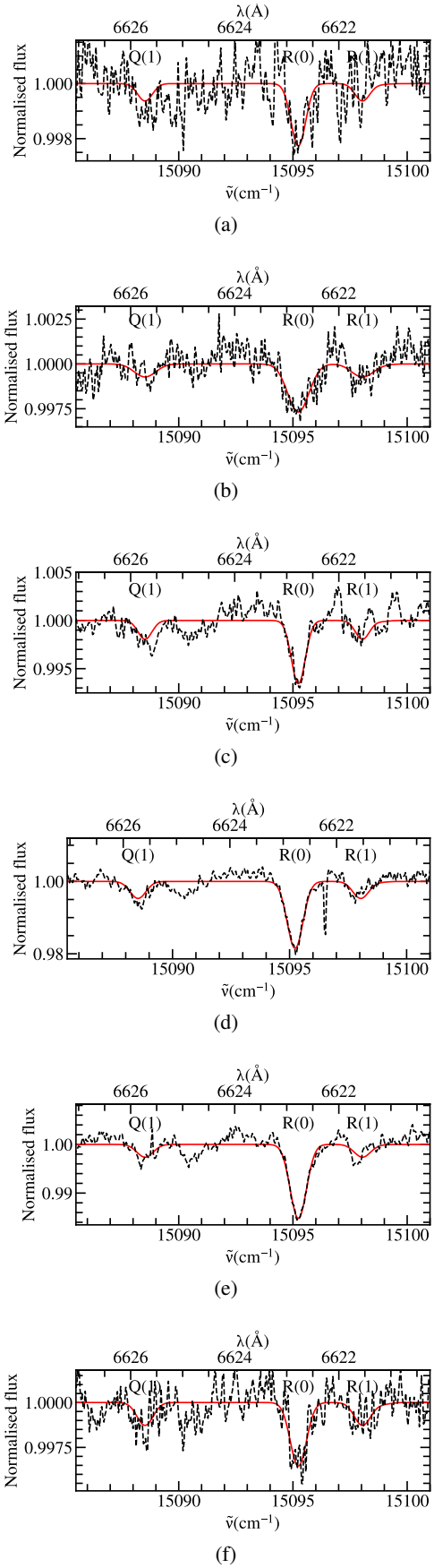

Fig. C.3. Fit of the HD 23180 (a), HD 24398 (b), HD 184915 (c), HD 185418 (d), HD 185859 (e), and HD 203532 (f) sight lines using a $\Sigma \rightarrow \Pi$ transition of a linear molecule model for the 6623 Å DIB system.

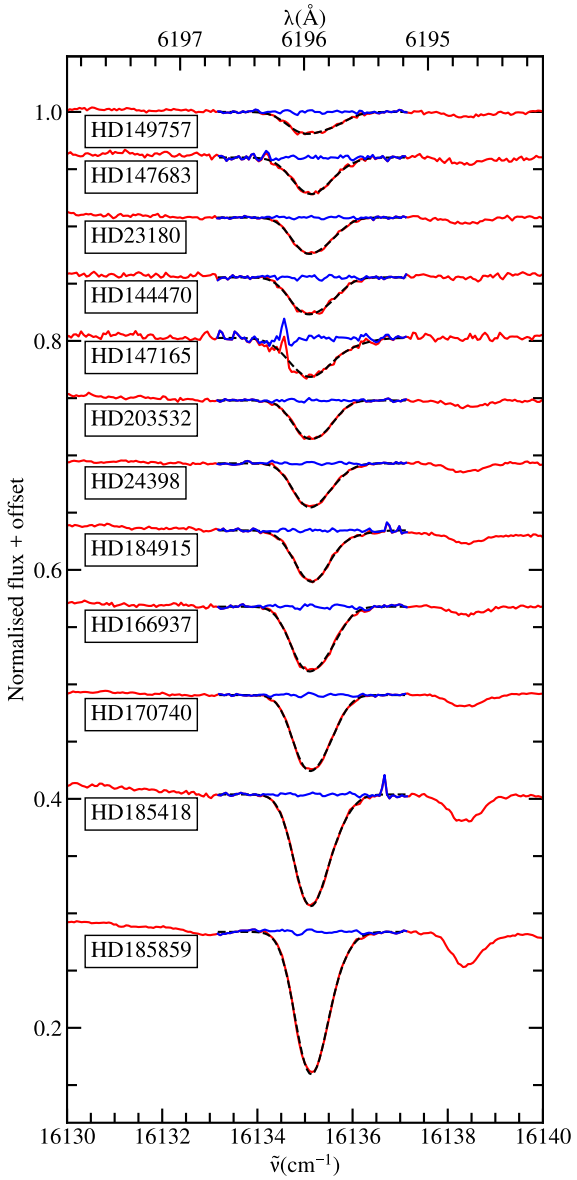

Fig. C.4. Double-Gaussian fit (dashed black) of the 6196 Å DIB in the spectra of our single cloud sight lines (red). The residual flux (blue) does not show significant systemic substructures of the 6196 Å DIB.

Appendix D: Deuterated DIB carrier candidates

A large number of candidates contains a deuterium atom, as can be seen in Table D.1. Deuterium might seem very unlikely due to its low abundance, but if some molecular formation channel is more efficient for deuterium than hydrogen, it cannot be excluded. With an abundance ratio of [D]/[H] $\approx 10^{-5}$ (Black & Dalgarno 1973), deuterium is still abundant compared to species other than hydrogen and helium. Deuterated molecules compared with hydrogenated molecules have lower zero-point energies due to the molecule's reduced mass being approximately doubled. This makes the deuterated molecule slightly more thermodynamically stable and is the underlying principle of fractionation in astrochemistry. And in cases such as N_2 (Heays, Alan N. et al. 2014), the fractionation can be photo-induced due to the slight differences in the photodissociation pathways that are slightly shifted by the change in zero-point energies in the heavier isotopologues. Especially for the anionic species, no experimental data was available from literature, but some neutrals could be ruled out as carriers. In a rotational analysis of the A-X band system of SrD, Appelblad & Barrow (1984) experimentally determined a rotational constant of $B'' = 1.86044(12)\,\mathrm{cm}^{-1}$ which is too far from our value of $B'' = 2.05 \pm 0.07\,\mathrm{cm}^{-1}$ for a $\Sigma \rightarrow \Sigma$ transition. For CaD, both B'' and B' are too large, and no transition is exactly at the observed energy, as measured experimentally by GharibNezhad et al. (2012). The experimentally measured rotational constants of MgD of $B'' = 3.0009462(11)\,\mathrm{cm}^{-1}$ (Lemoine et al. 1988), GaD of $B'' = 3.085\,\mathrm{cm}^{-1}$ (Lakshminarayana & Shetty 1987) and CrD of $B'' = 3.175443(21)\,\mathrm{cm}^{-1}$ (Ram & Bernath 1995) are too far from our observed values of the $\Sigma \rightarrow \Pi$ transitions with $B'' = 3.36 \pm 0.09\,\mathrm{cm}^{-1}$ (6623 Å DIB system) and $B'' = 3.47 \pm 0.12\,\mathrm{cm}^{-1}$ (6440 Å DIB system). Additionally, no matching transition wavelengths were found for those species. For ZnD, Ghazizadeh & Shayesteh (2017) found a matching rotational constant of $B'' = 3.35035973(26)\,\mathrm{cm}^{-1}$, but the lowest excited electronic state $A^2\Pi$ is at $T_v = 23387.6200(4)\,\mathrm{cm}^{-1}$ which is too high.

Table D.1. Rotational constants of proposed deuterated carrier molecules, same as Table 5.

Molecule	B'' (cm^{-1})	Molecular ground term	Lit.
SrD^-	1.66	$^1\Sigma^+$	...
KD	1.74	$^1\Sigma^+$	...
SrD	1.85	$^2\Sigma^+$	f[a]
CaD^-	1.97	$^1\Sigma^+$	...
YD^-	2.12	$^2\Sigma^+/^2\Pi$	...
CaD	2.18	$^2\Sigma^+$	f[b]
NaD^-	2.26	$^2\Sigma^+$	...
ZrD^-	2.27	$^3\Pi$	...
YD	2.32	$^1\Sigma^+$	...
MoD	2.91	$^6\Sigma^+$	...
TiD^+	3.01	$^3\Pi/^3\Sigma^-$	...
CrD^-	3.01	$^5\Sigma^+$	...
MgD	3.06	$^2\Sigma^+$	f[c]
GaD	3.17	$^1\Sigma^+$	f[d]
CrD	3.26	$^6\Sigma^+$	f[e]
(RhD^+)	3.40	$^4\Sigma^-/^4\Pi$	...
RuD	3.43	$^4\Sigma^-$	...
RuD^-	3.46	$^3\Sigma^-$	...
ZnD	3.49	$^2\Sigma^+$	f[f]
FeD^+	3.61	$^5\Sigma^+$	...
(RuD^+)	3.66	$^3\Sigma^-/^3\Pi$	...
CuD^-	3.70	$^2\Sigma^+$	...
CoD^+	3.81	$^4\Pi/^4\Sigma^-$	...
PdD^-	3.91	$^1\Sigma^+$	...
PdD^+	3.97	$^1\Sigma^+$	...

References. [a] Appelblad & Barrow (1984); [b] GharibNezhad et al. (2012); [c] Lemoine et al. (1988); [d] Lakshminarayana & Shetty (1987); [e] Ram & Bernath (1995); [f] Ghazizadeh & Shayesteh (2017)